

Drell-Yan production and Lam-Tung relation in the Color Glass Condensate formalism

François Gelis⁽¹⁾, Jamal Jalilian-Marian^(2,3)

August 2, 2018

1. Service de Physique Théorique (URA 2306 du CNRS)
CEA/DSM/Saclay, Bât. 774
91191, Gif-sur-Yvette Cedex, France
2. Institute for Nuclear Theory
University of Washington
Seattle, WA 98195-1550, USA
3. Department of Natural Sciences
Baruch College
New York, NY 10010, USA

Abstract

We study the Drell-Yan production cross section and structure functions in proton (deuteron)-nucleus collisions using the Color Glass Condensate formalism. The nucleus is treated in the Color Glass Condensate framework which includes both higher twist effects due to the inclusion of multiple scatterings and leading twist pQCD shadowing due to the small x resummation, while the proton (or deuteron) is treated within the DGLAP improved parton model. In particular, the Drell-Yan structure functions are used in order to investigate the Lam-Tung relation at small x , which is known to be identically zero at leading twist up to Next-to-Leading order, and is thus a good playground for studying higher twist effects. In agreement with this, we find that violations of this relation are more important for low momentum and invariant mass of the Drell-Yan pair, and also in the region of rapidity that corresponds to smaller values of x in the nucleus.

Preprint SPhT-T06/103

1 Introduction

The recent data from deuteron-gold collisions in the forward rapidity region at RHIC [1] have caused a great excitement in the high energy heavy ion physics community. The observed suppression of the hadron production transverse momentum spectrum in deuteron-gold collisions as compared to proton-proton collisions (normalized to the number of binary collisions) was qualitatively predicted by the saturation physics and the Color Glass Condensate formalism [2–5] and is now understood quantitatively using saturation based models [6–10].

While the produced hadron spectra in deuteron-gold collisions in mid rapidity can be described in terms of classical (Glauber like) multiple scattering [11–21], one needs to go beyond a simple multiple scattering picture in order to understand the suppression of the forward rapidity spectra. In the Color Glass Condensate formalism, this suppression is due to the evolution of the target nucleus wave function with x (or equivalently, with rapidity) described by the JIMWLK evolution equations [22–28,2–4] (or their large N_c limit known as the Balitsky-Kovchegov (BK) equation [29,30]).

To further probe the extend to which saturation is the dominant physics in the forward rapidity region at RHIC, and in order to clarify the role of the additional effects, such as parton recombination, cold matter energy loss, etc., which have recently been suggested [31–33] as the reason for the suppression pattern, it is essential to consider the electromagnetic probes of the Color Glass Condensate, such as photon and dilepton production [34–36] or photon-hadron correlations [37]. The Color Glass Condensate formalism would predict a similar suppression pattern for production of photons and dileptons while the parton recombination models should not since photons and dileptons do not interact strongly. Therefore, observation of (or lack thereof) a similar suppression in the production of photons (or dileptons) as in hadron production would firmly establish saturation as the underlying physics of the phenomena in the forward rapidity region at RHIC. In this paper we consider dilepton production in proton-nucleus collisions and provide quantitative predictions for Drell-Yan structure functions and angular correlations in the kinematic region appropriate for the PHENIX experiment at RHIC and CMS and ATLAS experiments at LHC [38].

2 Drell-Yan cross-section in the CGC formalism

2.1 Generalities

Electromagnetic observables (such as photons and dileptons) are cleaner probes of new phenomena than hadronic ones since they do not interact strongly and are not sensitive to the non-perturbative, and thus poorly understood, physics of hadronization. However they do suffer from the fact that their production rates is much smaller than the hadron production rate, due to smallness of the electromagnetic coupling constant, and that in case of photons, measuring them

precisely poses new experimental difficulties.

When looking for new physics effects, it helps enormously when the leading order processes which constitute the background vanish. This is the case for the so called Lam-Tung relation [39,40] in dilepton production in perturbative QCD. It is known that the Leading Order (LO) pQCD partonic cross sections satisfy the Lam-Tung relation. This is the analog of the Callan-Gross relation between the structure functions F_1 and F_2 in Deeply Inelastic Scattering (DIS) which reads $F_2 \equiv 2x F_1$ or alternatively, $F_L \equiv F_2 - 2x F_1 = 0$. This is an indication that the photon probe scatters off of a spin half object (a fermion) in the target and as such, helped establish quarks as the constituents of the target proton. The Callan-Gross relation is, however, not exact and receives α_s corrections due to radiation of gluons such that $F_L \sim \alpha_s xG(x, Q^2)$.

The Lam-Tung relation on the other hand does not receive any α_s corrections (the first correction is of order α_s^2) and therefore can be a very sensitive probe of new (beyond standard pQCD) physics, such as higher twists effects and/or a change from DGLAP to BFKL kinematics signified by the change of the anomalous dimension of the gluon distribution function. Here, we use the Color Glass Condensate formalism, which includes both the multiple scattering and BFKL anomalous dimension into effect, in order to investigate the possible beyond the standard pQCD physics in the Lam-Tung relation.

2.2 The cross-section and hadronic tensor

In [34] and [35], the expressions for photon and dilepton production cross sections in proton (deuteron)-nucleus collisions were derived, using a hybrid description in which the proton is described by ordinary parton distributions while the nucleus is described in terms of classical color sources and the color field they produce. In such a description, the leading process for the emission of a photon (real or virtual) is a quark coming from the proton, scattering off the classical color field of the nucleus, and radiating a photon. Two terms contribute to the production amplitude, depending on whether the photon is emitted before or after the scattering of the quark off the nucleus, as illustrated in figure 1. There

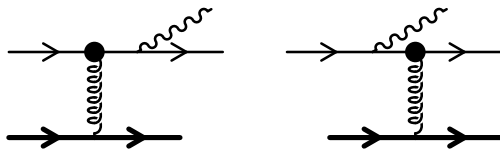


Figure 1: The two diagrams contributing to the emission of a photon in pA collisions. The black dot denotes the Wilson line that resums all the multiple scatterings of the quark off the color field of the nucleus.

could potentially be a third diagram, where the emission of the photon occurs inside the nucleus, so that the quark can interact with the nucleus before and

after the photon emission. However, such a contribution is suppressed by the inverse of the collision energy due to the Lorentz contraction of the nucleus.

If we denote p the momentum of the incoming quark, q the momentum of the outgoing quark, and k the momentum of the emitted photon, the amplitude for photon emission in a given configuration of the target color field reads [34,35] :

$$\begin{aligned} \mathcal{M}^\mu(\mathbf{p}|\mathbf{q}, k) &= 2\pi\delta(p^- - q^- - k^-) \int d^2\mathbf{x}_\perp e^{i(\mathbf{q}_\perp + \mathbf{k}_\perp - \mathbf{p}_\perp) \cdot \mathbf{x}_\perp} \left[V(\mathbf{x}_\perp) - 1 \right] \\ &\quad \times ee_q \bar{u}(\mathbf{p}) \left\{ \frac{\gamma^- (\not{q} + \not{k}) \gamma^\mu}{(q+k)^2} + \frac{\gamma^\mu (\not{p} - \not{k}) \gamma^-}{(p-k)^2} \right\} u(\mathbf{q}). \end{aligned} \quad (1)$$

In this formula, the nucleus is assumed to be moving in the positive z direction. We have neglected the mass of the quark, and e_q is the electrical charge of the quark in units of the electron charge e . $V(\mathbf{x}_\perp)$ is a Wilson line defined as follows :

$$V(\mathbf{x}_\perp) \equiv T_- \exp \left[-ig \int dz^- A_a^+(z^-, \mathbf{x}_\perp) t^a \right], \quad (2)$$

with t^a the generators of the fundamental representation of SU(3) and A_a^+ the classical color field of the nucleus in the color glass condensate description. In terms of the number density of color charges in the nucleus, $\rho_a(\mathbf{x}_\perp)$, its expression in the covariant gauge is :

$$A_a^+(x^-, \mathbf{x}_\perp) = -g\delta(x^-) \frac{1}{\partial_\perp^2} \rho_a(\mathbf{x}_\perp). \quad (3)$$

Turning this photon production amplitude into the amplitude for the production of a lepton pair, where the lepton has momentum k_1 and the anti-lepton has momentum k_2 ($k_1 + k_2 = k$), is straightforward. One simply needs to multiply it by the free propagator of a virtual photon, which in the Feynman gauge is $D_{\mu\nu}(k) = -ig_{\mu\nu}/k^2$, and by the leptonic current $J^\nu \equiv e\bar{v}(\mathbf{k}_2)\gamma^\nu u(\mathbf{k}_1)$. Therefore, the Drell-Yan amplitude is given by :

$$\begin{aligned} \mathcal{M}_{DY}(\mathbf{p}|\mathbf{q}, \mathbf{k}_1, \mathbf{k}_2) &= 2\pi\delta(p^- - q^- - k^-) \int d^2\mathbf{x}_\perp e^{i(\mathbf{q}_\perp + \mathbf{k}_\perp - \mathbf{p}_\perp) \cdot \mathbf{x}_\perp} \left[V(\mathbf{x}_\perp) - 1 \right] \\ &\quad \times ie^2 e_q \bar{u}(\mathbf{p}) \left\{ \frac{\gamma^- (\not{q} + \not{k}) \gamma^\mu}{(q+k)^2} + \frac{\gamma^\mu (\not{p} - \not{k}) \gamma^-}{(p-k)^2} \right\} u(\mathbf{q}) \frac{\bar{v}(\mathbf{k}_2)\gamma_\mu u(\mathbf{k}_1)}{(k_1 + k_2)^2}. \end{aligned} \quad (4)$$

It will be convenient to introduce a notation for the part of this amplitude that remains after we factor out the factor $2\pi\delta(p^- - q^- - k^-)$:

$$\mathcal{M}_{DY}(\mathbf{p}|\mathbf{q}, \mathbf{k}_1, \mathbf{k}_2) \equiv 2\pi\delta(p^- - q^- - k^-) M_{DY}(\mathbf{p}, \mathbf{q}; k_1, k_2). \quad (5)$$

Indeed, as was shown in [34], the cross-section for the process $qA \rightarrow ql^+l^-A$ is then given in terms of M_{DY} by the following formula :

$$\begin{aligned} d\sigma_{DY} &= \frac{1}{2p^-} \frac{d^2\mathbf{q}_\perp d^2q^-}{(2\pi)^3 2q^-} \frac{d^2\mathbf{k}_{1\perp} dk_1^-}{(2\pi)^3 2k_1^-} \frac{d^2\mathbf{k}_{2\perp} dk_2^-}{(2\pi)^3 2k_2^-} \\ &\quad \times 2\pi\delta(p^- - q^- - k_1^- - k_2^-) \frac{1}{N_c} \sum_{\text{colors}} \left\langle |M_{DY}(\mathbf{p}|\mathbf{q}, \mathbf{k}_1, \mathbf{k}_2)|^2 \right\rangle_A, \end{aligned} \quad (6)$$

where E_q , E_1 , and E_2 are respectively the energy of the final quark, of the lepton and of the anti-lepton. The bracket $\langle \dots \rangle_A$ denotes the average over the color sources in the target nucleus. We have summed over the colors of the final quark and averaged over the colors of the incoming quark. When we square the amplitude in order to obtain the cross-section, it is customary to write it in the following way :

$$d\sigma_{DY} = \frac{1}{(2\pi)^4} \frac{\alpha_{\text{em}}^2}{M^2} \frac{d^2\mathbf{k}_{1\perp} dk_1^-}{k_1^-} \frac{d^2\mathbf{k}_{2\perp} dk_2^-}{k_2^-} e_q^2 W_{\mu\nu} L^{\mu\nu} , \quad (7)$$

where M is the invariant mass of the lepton pair ($M^2 \equiv (k_1 + k_2)^2$), and $L^{\mu\nu}$ is a leptonic tensor coming from the trace over the Dirac indices in the lepton loop¹,

$$L^{\mu\nu} \equiv g^{\mu\nu} - \frac{k_1^\mu k_2^\nu + k_1^\nu k_2^\mu}{k_1 \cdot k_2} , \quad (8)$$

and where $W_{\mu\nu}$ contains the factors that depend on the nuclear target :

$$\begin{aligned} W_{\mu\nu} &= \frac{1}{2p^-} \int \frac{d^2\mathbf{q}_\perp dq^-}{(2\pi)^2 q^-} \delta(p^- - q^- - k^-) \int d^2\mathbf{x}_\perp d^2\mathbf{y}_\perp e^{i(\mathbf{q}_\perp + \mathbf{k}_\perp) \cdot (\mathbf{x}_\perp - \mathbf{y}_\perp)} \\ &\times \frac{1}{N_c} \text{tr} \left\langle \left[V(\mathbf{x}_\perp) - 1 \right] \left[V^\dagger(\mathbf{y}_\perp) - 1 \right] \right\rangle_A \text{tr} \left\{ \not{p} \left[\frac{\gamma^- (\not{q} + \not{k}) \gamma_\nu}{(q+k)^2} + \frac{\gamma_\nu (\not{p} - \not{k}) \gamma^-}{(p-k)^2} \right] \right. \\ &\quad \left. \times \not{q} \left[\frac{\gamma^- (\not{p} - \not{k}) \gamma_\mu}{(p-k)^2} + \frac{\gamma_\mu (\not{q} + \not{k}) \gamma^-}{(q+k)^2} \right] \right\} . \quad (9) \end{aligned}$$

In this formula, we denote $k \equiv k_1 + k_2$, and we have assumed that the incoming quark has no transverse momentum: $\mathbf{p}_\perp = 0$. Of course, the integration over the variable q^- is trivially done thanks to the delta function. Note that the first trace is over color indices while the second one is over the indices carried by the Dirac matrices.

By assuming translation invariance in the transverse plane for the nucleus, this formula may be rewritten in terms of the Fourier transform of the correlator of two Wilson lines :

$$\begin{aligned} W_{\mu\nu} &= \frac{\pi R_A^2}{2p^-(p^- - k^-)} \int \frac{d^2\mathbf{q}_\perp}{(2\pi)^2} C(\mathbf{q}_\perp + \mathbf{k}_\perp) \\ &\times \text{tr} \left\{ \not{p} \left[\frac{\gamma^- (\not{q} + \not{k}) \gamma_\nu}{(q+k)^2} + \frac{\gamma_\nu (\not{p} - \not{k}) \gamma^-}{(p-k)^2} \right] \right. \\ &\quad \left. \times \not{q} \left[\frac{\gamma^- (\not{p} - \not{k}) \gamma_\mu}{(p-k)^2} + \frac{\gamma_\mu (\not{q} + \not{k}) \gamma^-}{(q+k)^2} \right] \right\} . \quad (10) \end{aligned}$$

where we denote

$$\pi R_A^2 C(\mathbf{l}_\perp) \equiv \int d^2\mathbf{x}_\perp d^2\mathbf{y}_\perp e^{i\mathbf{l}_\perp \cdot (\mathbf{x}_\perp - \mathbf{y}_\perp)} \frac{1}{N_c} \text{tr} \langle V(\mathbf{x}_\perp) V^\dagger(\mathbf{y}_\perp) \rangle_A , \quad (11)$$

¹We also neglect the lepton mass.

R_A being the radius of the nucleus. The function $C(\mathbf{l}_\perp)$ is directly related to the Fourier transform of the cross-section for a $q\bar{q}$ dipole scattering on a target nucleus. Therefore, it could in principle be obtained from fits of Deep Inelastic Scattering on the same target. Note also that we have dropped terms with no Wilson lines, as well as terms with only one Wilson line. These terms have a $\delta(\mathbf{q}_\perp + \mathbf{k}_\perp)$ under the integral, and correspond to a situation where no transverse momentum is exchanged between the target nucleus and the quark line. They do not contribute to the photon production cross-section.

So far, we have written the Drell-Yan cross-section and structure functions for an incoming quark colliding on a nucleus. Naturally, they will be measured for incoming nucleons. The relation between the quantities defined in eqs. (7) and (9) for the quark-nucleus system and the equivalent quantities for the proton-nucleus system are :

$$\begin{aligned} d\sigma_{DY}^{\text{pA}} &= \int_0^1 dx_1 q(x_1, \mu^2) d\sigma_{DY}|_{p^- = x_1 \sqrt{s/2}} , \\ W_{\mu\nu}^{\text{pA}} &= \int_0^1 dx_1 q(x_1, \mu^2) e_q^2 W_{\mu\nu}|_{p^- = x_1 \sqrt{s/2}} , \end{aligned} \quad (12)$$

where x_1 is the longitudinal momentum fraction of the quark in the incoming nucleon. Note that the only combination of parton distributions of the proton that matter in this calculation is the structure function F_2 :

$$F_2(x_1, \mu^2) \equiv \sum_q e_q^2 q(x_1, \mu^2) , \quad (13)$$

since the ‘‘probe’’ with which we explore the proton is a photon. Most of our discussion will be about the structure functions of the quark-nucleus subsystem, and we will convolute them with the quark distribution of the proton (or deuteron in the case of RHIC) only at the end when we present numerical results.

2.3 Structure functions and the Lam-Tung relation

It is customary to perform a decomposition of the hadronic tensor $W_{\mu\nu}$ into four structure functions. There are a priori three 4-momenta upon which $W_{\mu\nu}$ might depend: P_1^μ, P_2^μ the momenta of the proton and of a nucleon in the nucleus respectively, and k^μ the momentum of the virtual photon. This tensorial decomposition is usually performed in the rest frame of the lepton pair, where $\mathbf{k} = 0$. Denoting E_1 and E_2 the energies of the proton and of a nucleon in the nucleus *in the rest frame of the lepton pair*², one first defines the following four

²The vectors $P_{1,2}^\mu$ should be kept in the center of momentum frame of the proton-nucleon subsystem, since it is in this frame that eq. (9) for $W_{\mu\nu}$ is defined.

projectors³ :

$$\begin{aligned}
P_{TL}^{\mu\nu} &\equiv -g^{\mu\nu} , & P_{L12}^{\mu\nu} &\equiv \frac{P_1^\mu P_2^\nu + P_1^\nu P_2^\mu}{E_1 E_2} , \\
P_{L1}^{\mu\nu} &\equiv \frac{P_1^\mu P_1^\nu}{E_1^2} , & P_{L2}^{\mu\nu} &\equiv \frac{P_2^\mu P_2^\nu}{E_2^2} .
\end{aligned} \tag{14}$$

From these projectors, one defines the following four structure functions :

$$\begin{aligned}
T_{TL} &\equiv P_{TL}^{\mu\nu} W_{\mu\nu} , & T_{L12} &\equiv P_{L12}^{\mu\nu} W_{\mu\nu} , \\
T_{L1} &\equiv P_{L1}^{\mu\nu} W_{\mu\nu} , & T_{L2} &\equiv P_{L2}^{\mu\nu} W_{\mu\nu} .
\end{aligned} \tag{15}$$

Alternatively, different sets of structure functions can be defined by applying a 4×4 “rotation matrix” to the previous set of structure functions. The helicity structure functions can be obtained in this way [41]. Several definitions of the helicity structure functions exist in the literature, and in this paper we are going to consider the so-called Collins-Soper structure functions, defined as :

$$\begin{bmatrix} W_{TL} \\ W_L \\ W_\Delta \\ W_{\Delta\Delta} \end{bmatrix} \equiv R_{CS} \begin{bmatrix} T_{TL} \\ T_{L1} \\ T_{L2} \\ T_{L12} \end{bmatrix} , \tag{16}$$

where the matrix R_{CS} is defined as :

$$R_{CS} \equiv \frac{1}{2} \begin{bmatrix} 1 & 0 & 0 & 0 \\ 0 & \frac{1}{2 \cos^2 \delta} & \frac{1}{2 \cos^2 \delta} & -\frac{1}{2 \cos^2 \delta} \\ 0 & -\frac{1}{\sin 2\delta} & \frac{1}{\sin 2\delta} & 0 \\ 1 & \frac{1+\cos^2 \delta}{\sin^2 2\delta} & -\frac{1+\cos^2 \delta}{\sin^2 2\delta} & \frac{1-3 \cos^2 \delta}{\sin^2 2\delta} \end{bmatrix} . \tag{17}$$

In this formula, we use the so-called “Collins-Soper frame” in order to define the angle δ : in the lepton pair rest frame, the momenta of the two incoming hadrons are not opposite, and the Z -axis is chosen to bisect the angle between P_1 and $-P_2$. δ is the angle between the Z -axis and the momentum P_1 , defined in figure (2) and given by

$$\cos^2 \delta = \frac{M^2}{M^2 + \mathbf{k}_\perp^2} , \quad \sin^2 \delta = \frac{\mathbf{k}_\perp^2}{M^2 + \mathbf{k}_\perp^2} . \tag{18}$$

³Note that, since these projectors are defined in terms of the ratios P_1^μ/E_1 and P_2^μ/E_2 , they are identical for the proton-nucleus system and for the quark-nucleus subsystem. This will become more obvious with the explicit formulas in eqs. (24), where one can see that the center of mass collision energy has disappeared. This means that we can perform these projections on the $W_{\mu\nu}$ of the qA subsystem, and convolute with the quark distribution of the proton only later.

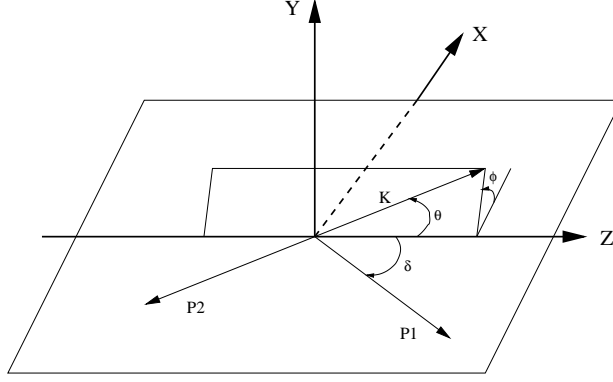


Figure 2: Definition of the angle δ .

For the sake of completeness, we also show the expressions for the structure functions explicitly,

$$\begin{aligned}
W_{TL} &= \frac{1}{2}T_{TL} , \\
W_L &= \frac{M^2 + \mathbf{k}_\perp^2}{4M^2} [T_{L1} + T_{L2} - T_{L12}] \\
W_\Delta &= \frac{1}{4} \frac{M^2 + \mathbf{k}_\perp^2}{Mk_\perp} [T_{L2} - T_{L1}] , \\
W_{\Delta\Delta} &= \frac{1}{2}T_{TL} - \frac{(M^2 + \mathbf{k}_\perp^2)(2M^2 + \mathbf{k}_\perp^2)}{8M^2\mathbf{k}_\perp^2} [T_{L1} + T_{L2}] \\
&\quad + \frac{(M^2 + \mathbf{k}_\perp^2)(-2M^2 + \mathbf{k}_\perp^2)}{8M^2\mathbf{k}_\perp^2} T_{L12} . \tag{19}
\end{aligned}$$

At leading twist, the following relation

$$\begin{aligned}
W_{\Delta\Delta} - \frac{1}{2}W_L &= \frac{1}{2} \left[T_{TL} - \frac{(M^2 + k_t^2)^2}{2M^2k_t^2} (T_{L1} + T_{L2}) - \frac{M^4 - k_t^4}{2M^2k_t^2} T_{L12} \right] \\
&= 0 , \tag{20}
\end{aligned}$$

known as the *Lam-Tung relation* [39,40], is valid up to Next-to-Leading order, i.e. up to the order $\mathcal{O}(\alpha_s)$.

2.4 Kinematics and matrix elements

Below we will discuss violations of this relation in the kinematics appropriate to the RHIC and LHC experiments. Before that, it is instructive to be more specific. The vectors P_1^μ and P_2^μ are proportional to unit vectors along the light

cones⁴ :

$$P_1^\mu = \sqrt{\frac{s}{2}} v_-^\mu, \quad P_2^\mu = \sqrt{\frac{s}{2}} v_+^\mu, \quad (21)$$

with

$$v_+^\mu \equiv \frac{1}{\sqrt{2}}(1, 0, 0, 1), \quad v_-^\mu \equiv \frac{1}{\sqrt{2}}(1, 0, 0, -1). \quad (22)$$

(Remember that the proton is moving in the negative z direction and the nucleus in the positive z direction). The energies E_1 and E_2 of the proton and of a nucleon of the nucleus are, in the rest frame of the lepton pair,

$$E_1 = \frac{e^{-y}}{2M} \sqrt{s(M^2 + \mathbf{k}_\perp^2)}, \quad E_2 = \frac{e^{+y}}{2M} \sqrt{s(M^2 + \mathbf{k}_\perp^2)}, \quad (23)$$

so that the projectors of eqs. (14) can be rewritten as :

$$\begin{aligned} P_{TL}^{\mu\nu} &\equiv -g^{\mu\nu}, & P_{L12}^{\mu\nu} &\equiv \frac{2M^2}{M^2 + \mathbf{k}_\perp^2} [v_+^\mu v_-^\nu + v_+^\nu v_-^\mu], \\ P_{L1}^{\mu\nu} &\equiv \frac{2M^2 e^{+2y}}{M^2 + \mathbf{k}_\perp^2} v_-^\mu v_-^\nu, & P_{L2}^{\mu\nu} &\equiv \frac{2M^2 e^{-2y}}{M^2 + \mathbf{k}_\perp^2} v_+^\mu v_+^\nu. \end{aligned} \quad (24)$$

Performing explicitly the Dirac algebra and the contractions with these projectors, we obtain the following expression for the four T 's :

$$T_\alpha = \frac{\pi R_A^2}{2(1-z)} \int \frac{d^2 \mathbf{q}_\perp}{(2\pi)^2} C(\mathbf{q}_\perp + \mathbf{k}_\perp) \mathcal{T}_\alpha, \quad (25)$$

where $\alpha \in \{TL, L1, L2, L12\}$ with

$$\begin{aligned} \mathcal{T}_{TL} &= 16 \left\{ \frac{(1-z)k_\perp^2}{[M^2 - 2p \cdot k]^2} + \frac{[z\mathbf{q}_\perp - (1-z)\mathbf{k}_\perp]^2}{(1-z)[M^2 + 2q \cdot k]^2} \right. \\ &\quad \left. - 2 \frac{[(1-z)q_\perp^2 + (2-z)\mathbf{q}_\perp \cdot \mathbf{k}_\perp]}{[M^2 - 2p \cdot k][M^2 + 2q \cdot k]} \right\}, \\ \mathcal{T}_{L1} &= \frac{32(1-z)}{z^2} M^2 \left\{ \frac{1}{M^2 + 2q \cdot k} + \frac{1-z}{M^2 - 2p \cdot k} \right\}^2, \\ \mathcal{T}_{L2} &= \frac{32z^2}{1-z} \frac{M^2}{(M^2 + \mathbf{k}_\perp^2)^2} \left\{ \frac{q_\perp^2 (\mathbf{q}_\perp + \mathbf{k}_\perp)^2}{[M^2 + 2q \cdot k]^2} \right\}, \\ \mathcal{T}_{L12} &= 64 \frac{M^2}{M^2 + \mathbf{k}_\perp^2} \frac{\mathbf{q}_\perp \cdot (\mathbf{q}_\perp + \mathbf{k}_\perp)}{[M^2 + 2q \cdot k]} \left\{ \frac{1-z}{M^2 - 2p \cdot k} + \frac{1}{M^2 + 2q \cdot k} \right\}. \end{aligned} \quad (26)$$

⁴We can afford to be a bit sloppy here about the use of the squared center of mass energy for the proton-nucleus system, s , instead of that for the quark-nucleus subsystem, $\hat{s} = x_1 s$. Indeed, since the energies E_1 and E_2 are also proportional to \sqrt{s} , this choice is irrelevant in the definition of the projectors.

Eqs. (25) and (26) thus provide the full leading result for the production of a lepton pair in proton-nucleus collisions in the CGC framework. These results are for a quark with a fixed longitudinal momentum p^- . In order to obtain the corresponding results for an incoming proton, one needs simply to convolute with the quark distribution $q(x_1)$, and use eqs. (26) with $z = k^-/(x_1\sqrt{s/2})$.

This result is of the same order in α_s as the standard NLO $qg \rightarrow q\gamma^* \rightarrow q\ell^+\ell^-$ contribution, but compared to the standard pQCD result it resums all the multiple scatterings on the dense nucleus. One point should be emphasized: our calculation incorporates also the ‘‘LO’’ process $q\bar{q} \rightarrow \gamma^* \rightarrow \ell^+\ell^-$, although in a non obvious way. Indeed, the intermediate – virtual and space-like – quark in the diagrams of figure (1) must be interpreted in some kinematical domain as an antiquark belonging to the wave-function of the nucleus (in that case, the quark in the final state came also from the nucleus wave-function). Note however the pQCD NLO process $q\bar{q} \rightarrow g\gamma^* \rightarrow g\ell^+\ell^-$ would only appear at the next order in our calculation, via diagrams similar to those of figure (1) but with a gluon in the final state in addition to the photon. In order to understand why this process does not appear on the same footing here, one has to remember that in our approach the antiquarks are produced explicitly from the gluons, and that a process that has both an antiquark in the initial state and a gluon in the final state is non-leading in our framework.

2.5 The collinear factorization limit

In eq. (10), the function $C(\mathbf{q}_\perp + \mathbf{k}_\perp)$ resums all the multiple scatterings that the quark undergoes while it goes through the nucleus. However, it is possible to extract from this formula the contribution from a single scattering, i.e. the leading-twist contribution. In this limit, one should recover the results from collinear factorization in perturbative QCD.

This is done as follows. One assumes that the momentum scales $\mathbf{q}_\perp, \mathbf{k}_\perp, M$ that characterize the final state are much larger than the saturation scale, and one makes the approximation that the transverse momentum of the incoming gluons, $\mathbf{l}_\perp = \mathbf{q}_\perp + \mathbf{k}_\perp$, is large compared to Q_s but small compared to the scales of the final state. This approximation is legitimate in this regime, because when there is a large range between Q_s and the scales of the final state, the integration over \mathbf{l}_\perp is dominated by a large logarithmic contribution that comes from values of \mathbf{l}_\perp comprised in this range. One must first approximate the matrix elements \mathcal{T}_α by assuming that the transverse momentum of the gluons coming from the nucleus, $\mathbf{l}_\perp \equiv \mathbf{q}_\perp + \mathbf{k}_\perp$, is smaller than the other scales. As pointed out after eq. (10), these matrix elements vanish when $\mathbf{l}_\perp = 0$, and therefore one should keep higher orders in the expansion in \mathbf{l}_\perp . Formally, one can write :

$$\mathcal{T}_\alpha = \mathbf{A}_\alpha^i \mathbf{l}_\perp^i + \mathbf{B}_\alpha^{ij} \mathbf{l}_\perp^i \mathbf{l}_\perp^j + \dots \quad (27)$$

Since the function $C(\mathbf{l}_\perp)$ depends only on the modulus of the vector \mathbf{l}_\perp but not on its orientation, the term linear in \mathbf{l}_\perp in this expansion will vanish when inserted into eq. (25) when we perform the integration over the orientation of

the vector \mathbf{l}_\perp . We therefore need to expand the \mathcal{T}_α 's to second order in \mathbf{l}_\perp . Assuming this expansion has been performed, we can now write

$$T_\alpha \approx \frac{\pi R_A^2}{4(1-z)} B_\alpha^{ii} \int \frac{d^2 \mathbf{l}_\perp}{(2\pi)^2} l_\perp^2 C(l_\perp), \quad (28)$$

Recalling the fact that in the leading-twist limit – valid here since $l_\perp \gg Q_s^-$, $l_\perp^2 C(l_\perp)$ is proportional to the non-integrated gluon distribution of the nucleus, the integral over \mathbf{l}_\perp that appears in the previous equation gives the usual integrated gluon distribution, $xG_A(x, Q^2)$, with a resolution scale Q^2 which is the upper limit of the range of validity of the expansion in eq. (27).

It is straightforward to perform explicitly the expansion in powers of \mathbf{l}_\perp of the matrix elements \mathcal{T}_α , in order to obtain the second order coefficients B_α^{ii} . One gets :

$$\begin{aligned} B_{L1}^{ii} &= 128 z^2 (1-z)^3 \frac{M^2 \mathbf{k}_\perp^2}{[\mathbf{k}_\perp^2 + (1-z)M^2]^4}, \\ B_{L2}^{ii} &= 64 z^4 (1-z) \frac{M^2 \mathbf{k}_\perp^2}{(\mathbf{k}_\perp^2 + M^2)^2 [\mathbf{k}_\perp^2 + (1-z)M^2]^2}, \\ B_{L12}^{ii} &= -128 z^3 (1-z)^2 \frac{M^2 \mathbf{k}_\perp^2}{(\mathbf{k}_\perp^2 + M^2) [\mathbf{k}_\perp^2 + (1-z)M^2]^3}, \\ B_{TL}^{ii} &= 32 z^2 (1-z) \frac{1}{[\mathbf{k}_\perp^2 + (1-z)M^2]^4} \\ &\quad \times [4(1-z)^2 \mathbf{k}_\perp^2 M^2 + [1 + (1-z)^2][\mathbf{k}_\perp^4 + (1-z)^2 M^4]]. \end{aligned} \quad (29)$$

Using these expressions, it is easy to verify that the Lam-Tung sum rule given in eq. (20) holds identically in the leading twist (single scattering) limit.

2.6 Angular coefficients

Based on the general Lorentz structure of the cross section, one can write the transverse momentum integrated Drell-Yan cross section in terms of the polar and azimuthal angles of the dilepton pair in the dilepton center of mass frame as

$$\frac{dN}{d\Omega} \equiv \left[\frac{d\sigma}{d^4 k} \right]^{-1} \frac{d\sigma}{d\Omega d^4 k} \quad (30)$$

where $d\Omega \equiv d\cos\theta d\phi$ is the solid angle, with θ and ϕ defined in Fig. (2) and k is the dilepton four momentum with

$$\begin{aligned} \frac{dN}{d\Omega} &= \frac{3}{16\pi W_{TL}} \left[W_{TL} (1 + \cos^2 \theta) + \frac{1}{2} W_L (1 - 3 \cos^2 \theta) \right. \\ &\quad \left. + W_\Delta \sin 2\theta \cos \phi + W_{\Delta\Delta} \sin^2 \theta \cos 2\phi \right]. \end{aligned} \quad (31)$$

It is customary to parameterize this cross-section in terms of the angular coefficients A_0, A_1, A_2 as follows,

$$\frac{dN}{d\Omega} = \frac{3}{16\pi} \left[1 + \cos^2 \theta + \frac{1}{2} A_0 (1 - 3 \cos^2 \theta) + A_1 \sin 2\theta \cos \phi + \frac{1}{2} A_2 \sin^2 \theta \cos 2\phi \right], \quad (32)$$

so that

$$A_0 \equiv \frac{W_L}{W_{TL}}, \quad A_1 \equiv \frac{W_\Delta}{W_{TL}}, \quad A_2 \equiv \frac{2W_{\Delta\Delta}}{W_{TL}} \quad (33)$$

in terms of which the Lam-Tung relation simply reads $A_0 = A_2$. Below we will show our results for the structure functions W 's as well as the angular parameters A 's.

3 The dipole cross-section

3.1 Balitsky-Kovchegov equation

All single inclusive particle production cross sections in the Color Glass Condensate formalism depend on the Fourier transform $C(l_\perp)$ of the dipole cross section⁵, which is the probability for scattering of a high energy quark-antiquark dipole on a target. The dipole cross section evolves with rapidity according to the JIMWLK equation, so that given the dipole profile at some initial point x_0 , the dependence of the cross section on x (or rapidity) can be in principle obtained from the JIMWLK equation. In practice, this is very difficult to do (see [42]) and it is much simpler to use an approximate form of this evolution – known as the BK equation [29,30] – which can be obtained from the JIMWLK equation as a mean field approximation in the large N_c limit. Here we will use the numerical solution of the BK equation in order to investigate the properties of the Drell-Yan structure functions.

In momentum space, the BK equation takes the form

$$\frac{\partial T(k_\perp, Y)}{\partial Y} = \bar{\alpha}_s (K \otimes T)(k_\perp, Y) - \bar{\alpha}_s T^2(k_\perp, Y), \quad (34)$$

where we denote $\bar{\alpha}_s \equiv \alpha_s N_c / \pi$. The operator K is the well known BFKL kernel in momentum space [43,44], whose action on the function T is given by

$$(K \otimes T)(k_\perp, Y) \equiv \int_0^{+\infty} \frac{d(k'_\perp{}^2)}{k'_\perp{}^2} \left\{ \frac{k'_\perp{}^2 T(k'_\perp, Y) - k_\perp^2 T(k_\perp, Y)}{|k_\perp^2 - k'_\perp{}^2|} + \frac{k_\perp^2 T(k_\perp, Y)}{\sqrt{4k'_\perp{}^4 + k_\perp^4}} \right\}. \quad (35)$$

⁵Note that in case of gluon scattering one has a dipole in the adjoint representation.

The function $T(k_\perp, Y)$ is the Bessel-Fourier transform of the dipole-target scattering amplitude $T(r_\perp, Y)$:

$$T(k_\perp, Y) = \int_0^{+\infty} \frac{dr_\perp}{r_\perp} J_0(k_\perp r_\perp) T(r_\perp, Y), \quad (36)$$

where r_\perp is the size of the $q\bar{q}$ dipole and k_\perp is its conjugate transverse momentum. The dipole amplitude T is defined in terms of the correlator of two Wilson lines of gauge fields in the target as

$$T(r_\perp, Y) = 1 - \frac{1}{N_c} \text{Tr} \langle V^\dagger(0) V(\mathbf{r}_\perp) \rangle_Y, \quad (37)$$

where we have assumed translation invariance in the transverse plane in order to set the quark transverse coordinate to 0. The scattering amplitude T is related to the function $C(\mathbf{l}_\perp)$ by

$$C(\mathbf{l}_\perp) \equiv \int d^2\mathbf{r}_\perp e^{i\mathbf{l}_\perp \cdot \mathbf{r}_\perp} [1 - T(\mathbf{r}_\perp, Y)]. \quad (38)$$

Therefore, in order to obtain the function $C(\mathbf{l}_\perp)$ needed in the evaluation of the Drell-Yan structure functions, we must first solve the BK equation 34 for $T(k_\perp, Y)$, then invert eq. (36) in order to obtain $T(r_\perp, Y)$, and finally obtain $C(\mathbf{l}_\perp)$ by a Fourier transform.

The BK equation must be supplemented by an initial condition at $Y = 0$, for which we take the value of $T(k_\perp)$ predicted by the MV model [45–47] with an initial saturation momentum of $Q_s^2 = 2 \text{ GeV}^2$. This initial condition is assumed to correspond to an x_2 in the nucleus of $x_2^0 \equiv 10^{-2}$, which means that the parameter Y in $T(r_\perp, Y)$ should be interpreted as $Y = \ln(x_2^0/x_2)$. For values of x_2 larger than x_2^0 , we use the following naive extrapolation :

$$C(\mathbf{l}_\perp, x_2) = \left(\frac{1 - x_2}{1 - x_2^0} \right)^4 C(\mathbf{l}_\perp, x_2^0). \quad (39)$$

The idea behind this extrapolation is that the unintegrated gluon distribution that appears in the gluon yield (see [18]) is proportional to $C(\mathbf{l}_\perp)$, and should vanish like $(1 - x_2)^4$ when x_2 approaches 1 (the exponent 4 comes from quark counting rules).

Note also that we solve the BK equation with a fixed value of the coupling constant α_s . However, we set it to a rather low value in order to correctly reproduce the rate of growth of the saturation scale, as inferred for instance from the study of geometrical scaling at HERA [48]. This approach has already led to good results in the analysis of limiting fragmentation in [49].

3.2 Models of the dipole cross section

As an alternative to solving the BK equation, one can model the behavior of the dipole cross section based on its known properties. These phenomenological

models have been used to investigate particle production at RHIC and LHC as well as structure functions in Deeply Inelastic Scattering in HERA. Here we will use two of these models, known as the KKT [7] and DHJ [9,10] parameterizations, to calculate rapidity and transverse momentum dependence of the Drell-Yan structure functions in the kinematics appropriate for RHIC and LHC.

The KKT parameterization of the dipole cross section was quite successful in description of the forward rapidity hadron production cross section in deuteron-gold collisions at RHIC. In this parameterization, the dipole forward amplitude is modeled as

$$T(\mathbf{r}_\perp, Y) = 1 - \exp \left[-\frac{1}{4} [r_\perp^2 Q_s^2(Y)]^{\gamma(r_\perp, Y)} \right]. \quad (40)$$

In the KKT parameterization, the anomalous dimension $\gamma(r_\perp, Y)$ is given by

$$\gamma(r_\perp, Y) = \frac{1}{2} \left(1 + \frac{\xi(r_\perp, Y)}{\xi(r_\perp, Y) + \sqrt{2\xi(r_\perp, Y)} + 28\zeta(3)} \right) \quad (41)$$

and

$$\xi(r_\perp, Y) \equiv \frac{\log(1/r_\perp^2 Q_0^2)}{(\lambda/2)(Y - Y_0)}. \quad (42)$$

The saturation scale is given by $Q_s(Y) = Q_0 \exp[\lambda(Y - Y_0)/2]$ with $Y = \ln 1/x_2$ and $Y_0 = 0.6$, $\lambda = 0.3$. While the KKT parameterization of the dipole cross section was the first one to reproduce quantitatively the forward rapidity RHIC data, it has some shortcomings. For example, the assumed dependence of the anomalous dimension on r_\perp (or equivalently k_\perp) is too flat as shown in [9].

In the DHJ parameterization [9,10] of the dipole cross section, the anomalous dimension is given instead by

$$\gamma(r_\perp, Y) \equiv \gamma_s + (1 - \gamma_s) \frac{\log(1/r_\perp^2 Q_s^2)}{\lambda Y + \log(1/r_\perp^2 Q_s^2) + d\sqrt{Y}} \quad (43)$$

with $\gamma_s \simeq 0.62$, and $d = 1.2$. This model has the advantage that it accounts for the more rapid change of the anomalous dimension with transverse size (or momentum) which is needed in order to quantitatively describe the hadron transverse momentum spectra in both forward and mid rapidity deuteron-gold collisions at RHIC. For further details of the two models and their applications to RHIC data, we refer the reader to [9,10]. In the following we do not consider the KKT model any further, and we use either the BK evolution equation or the DHJ model.

4 Numerical results

4.1 Kinematics

Let us complete the eqs. (26) by some useful formulas for the denominators that appear in the \mathcal{T}_α 's :

$$\begin{aligned} M^2 - 2p \cdot k &= M^2 - \frac{M^2 + k_\perp^2}{z}, \\ M^2 + 2q \cdot k &= \frac{M^2}{z} + \frac{(z\mathbf{q}_\perp - (1-z)\mathbf{k}_\perp)^2}{z(1-z)}, \end{aligned} \quad (44)$$

where we recall that the variable z is defined as $z = k^-/p^-$. These formulas highlight the fact that the \mathcal{T}_α 's defined in eqs. (26) depend on the parameters M, \mathbf{k}_\perp, y of the virtual photon, on the transverse momentum \mathbf{q}_\perp of the outgoing quark, and on the momentum fraction z of the photon relative to the incoming quark. In particular, this variable z is the only reference to the momentum of the incoming quark in these formulas.

For an incoming quark carrying the fraction x_1 of the longitudinal momentum of the proton, we also have :

$$zx_1 = \sqrt{\frac{M^2 + k_\perp^2}{s}} e^{-y}. \quad (45)$$

Note that since both z and x_1 must be smaller than unity, this implies obvious limits to the phase-space allowed for the produced virtual photon, since we must have :

$$x_1^{\min} \equiv \sqrt{\frac{M^2 + k_\perp^2}{s}} e^{-y} \leq 1. \quad (46)$$

The notation for this quantity comes from the fact that it is also the minimal allowed value of x_1 . Thus, the structure function T_α for the proton-nucleus system can be written as

$$T_\alpha^{\text{pA}} = \int_{x_1^{\min}}^1 dx_1 q(x_1, \mu^2) \frac{\pi R_A^2}{2(1 - \frac{x_1^{\min}}{x_1})} \int \frac{d^2\mathbf{q}_\perp}{(2\pi)^2} C(\mathbf{q}_\perp + \mathbf{k}_\perp, x_2) \mathcal{T}_\alpha \left(z = \frac{x_1^{\min}}{x_1} \right). \quad (47)$$

One last point remains to be clarified: the dependence of the function C on x_2 is now explicitly shown. This dependence arises from the renormalization group resummation of small x effects via JIMWLK equations and has the interpretation as the longitudinal momentum fraction at which the nucleus is probed. It can be evaluated as

$$x_2 \equiv \frac{k^+ + q^+}{\sqrt{s/2}} = x_1^{\min} e^{2y} + \frac{q_\perp^2}{s(x_1 - x_1^{\min})}. \quad (48)$$

Note that the minimal value of x_2 is

$$x_2^{\min} = \sqrt{\frac{M^2 + k_\perp^2}{s}} e^{+y}, \quad (49)$$

(With our choice to have the nucleus moving in the $+z$ direction, small values of x_2 are reached when the photon rapidity is negative.) and that the relation between x_1 and x_2 is more symmetric if written as :

$$(x_1 - x_1^{\min})(x_2 - x_2^{\min}) = \frac{q_{\perp}^2}{s}. \quad (50)$$

Moreover, we can if necessary replace the integration over x_1 in eq. (47) by an integration over x_2 by noting that

$$\frac{dT_{\alpha}^{\text{pA}}}{dx_2 d^2 \mathbf{q}_{\perp}} = \frac{x_1 - x_1^{\min}}{x_2 - x_2^{\min}} \frac{dT_{\alpha}^{\text{pA}}}{dx_1 d^2 \mathbf{q}_{\perp}}. \quad (51)$$

This is useful in order to determine what are the values of x_2 that contribute the most to the Drell-Yan structure functions.

4.2 x_1 and x_2 dependence of the integrand

Let us first study the x_1 and x_2 dependence of the integrand. We do this for pA collisions at the LHC center of mass energy, i.e. $\sqrt{s} = 8.8$ TeV, for nuclei with $A^{1/3} = 6$. In figure 3, we display the x_1 dependence for the four W 's (i.e. we have multiplied eq. (47) by the rotation matrix R_{CS} given in eq. (17)), for $k_{\perp} = M = 3$ GeV and $y = -3$. We use the CTEQ6 (see [50] for details) set of parton distributions for the quark and antiquark distributions of the proton. In this figure, we compare the x_1 dependence that results from the BK evolution of the dipole cross-section, and from the DHJ model. As one can see, the two models lead to results that are very similar: the largest contributions come from values of x_1 immediately above the minimal value x_1^{\min} , and the integrand drops very quickly as x_1 increases. One can also note that the integrand for W_{Δ} vanishes and changes sign at some intermediate value of x_1 (for this integrand, we have displayed its absolute value, hence the cusp at the location of the zero on the logarithmic plot). In fact, for the kinematical parameters of the virtual photon used here, the two descriptions of the dipole cross-sections are very close even quantitatively. However, as we shall see later, this is not the case everywhere.

In figure 4, we have used the eq. (51) in order to display the x_2 dependence of the same integrands. In order to see how the dominant values of x_2 vary with the photon rapidity, we have considered three values of y , $y = -6, -3$ and 0 (the first one can be reached only by the CMS and ATLAS detectors, while the last two may also be studied by ALICE). To avoid overcrowding the figure, we display the results of this study only in the case of the BK evolution⁶. As in the case of the x_1 dependence, the dominant values of x_2 are located just above the minimal value x_2^{\min} , and the integrand decreases quickly as x_2 increases.

⁶At $x_2 = 10^{-2}$, one can notice a very small discontinuity in the slope of all the curves. This is the value of x_2 where we switch to the extrapolation described by eq. (39). As long as this point is far from x_2^{\min} , this extrapolation will not affect significantly the result of the integration over x_2 .

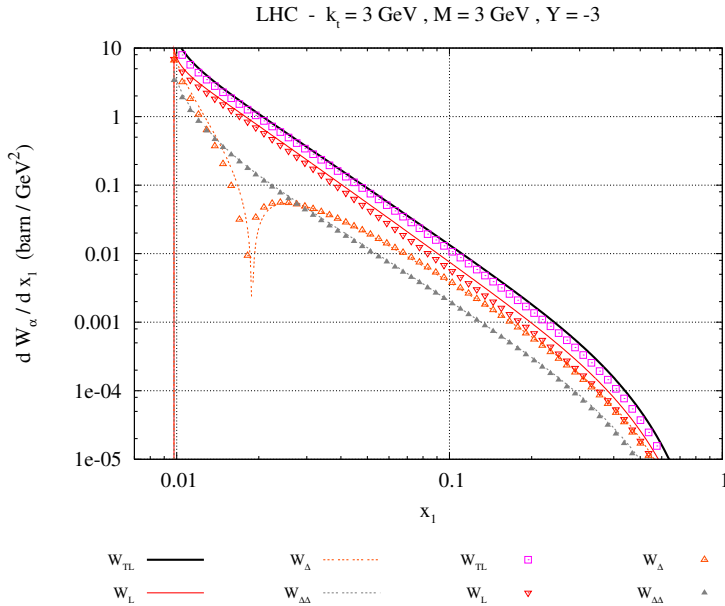


Figure 3: x_1 dependence of the integrand for the W 's. The kinematical parameters of the virtual photons are $k_{\perp} = 3 \text{ GeV}$, $M = 3 \text{ GeV}$ and $y = -3$, and the center of mass energy is $\sqrt{s} = 8.8 \text{ TeV}$. Lines: BK evolution. Points: DHJ model.

This enables one to select different windows in x_2 by varying the kinematical parameters of the virtual photon. This is illustrated in figure 4 with three different values of the photon rapidity. As one can see, it is possible to explore very small values of x_2 by going to negative rapidities, provided that the photon transverse momentum and invariant mass remain rather small.

4.3 Structure functions for pA and dA collisions

4.3.1 k_{\perp} dependence

Let us now display the results for the W 's, integrated over the momentum fraction x_1 of the incoming quark. We have performed this calculation both for the LHC and for RHIC. For the latter, we have used a center of mass energy $\sqrt{s} = 200 \text{ GeV}$ and the incoming projectile is taken to be a deuteron⁷ rather

⁷The CTEQ package does not provide parton distributions for the deuteron. In order to overcome this restriction, we assume that one can just add the parton distributions of a proton and of a neutron, i.e. we neglect the shadowing that may occur in the deuteron. This is a rather good assumption as long as x_1 is not too small. In order to obtain the quark distributions in the neutron, we just exchange the u and d valence distributions of a proton, and we assume that the sea quark distributions are identical in a proton and a neutron.

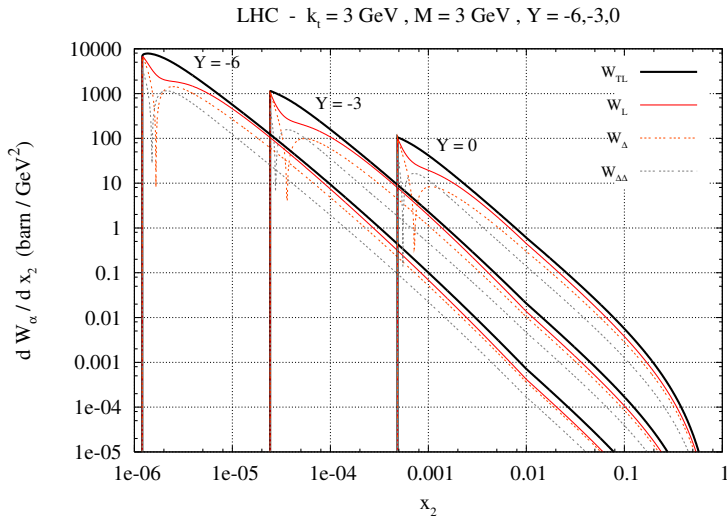


Figure 4: x_2 dependence of the integrand for the W 's, with the BK evolution. The kinematical parameters of the virtual photons are $k_{\perp} = 3 \text{ GeV}$, $M = 3 \text{ GeV}$ and we consider the rapidities $y = -6, -3$ and 0 . The center of mass energy is $\sqrt{s} = 8.8 \text{ TeV}$.

than a proton.

In figure 5, we display the dependence of the Drell-Yan structure functions on the transverse momentum of the virtual photon, for a fixed invariant mass and rapidity (this rapidity is chosen negative to be in the region where the nucleus is explored at small x_2). The calculation has been performed with the function $C(\mathbf{l}_{\perp}, x_2)$ resulting from the BK evolution (lines) and from the DHJ model (points), both for the LHC (left) and for RHIC (right). We also display on the same plot the difference $W_{\Delta\Delta} - W_L/2$, which is expected to vanish if the Lam-Tung relation is satisfied. Since we have checked explicitly that this combination vanishes identically in the leading twist approximation, any non-zero value for this quantity is due to higher twist corrections – i.e. to multiple scatterings of the quark in the nuclear target. One can see in figure 5 that the BK evolution and the DHJ model lead to qualitatively similar features in the Drell-Yan structure functions. The difference between the two descriptions is never very large (at most a factor 3), but one can see that it is more pronounced at large k_{\perp} , and also more pronounced at RHIC energy compared to LHC energy. Moreover, the fact that the W 's obtained with the DHJ model drop slightly faster at large k_{\perp} than those obtained from the BK evolution suggests that the difference comes from the anomalous dimension γ . In the BK evolution, it is always slightly above $1/2$, while the DHJ parameterization is such that this anomalous dimension goes back to unity at large momentum.

Note that the difference $W_{\Delta\Delta} - W_L/2$ should be compared to the structure

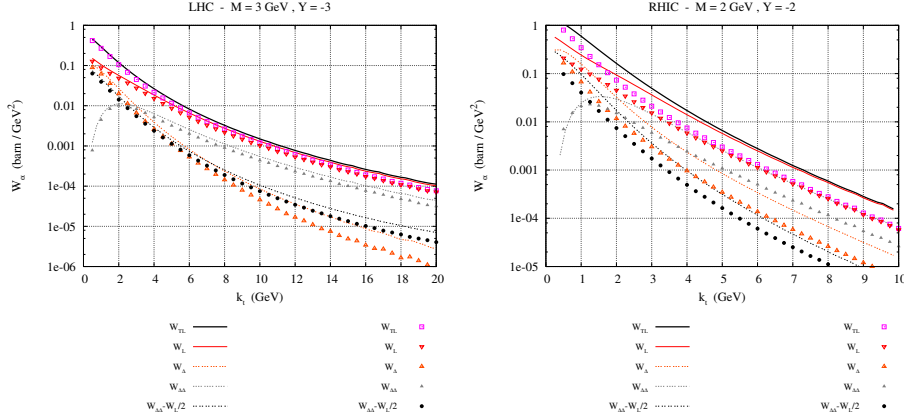


Figure 5: Drell-Yan structure functions as a function of k_{\perp} , for RHIC (right) and LHC (left). Lines: BK evolution. Points: DHJ model.

function W_{TL} (indeed, the W_{TL} structure function, obtained by contracting with $g^{\mu\nu}$, is closely related to the *total* cross-section). One sees that this combination is more and more suppressed as the transverse momentum of the virtual photon increases, as expected for a higher twist quantity. This means that violations of the Lam-Tung relation should be searched at low k_{\perp} rather than at large k_{\perp} . In figure 6, we display the angular coefficients defined in section 2.6 for the same set of parameters. Violations of the Lam-Tung relation should be visible in the fact that the difference $A_0 - A_2$ is non-zero. One can see that they decrease, albeit very slowly, when the transverse momentum increases.

4.3.2 M dependence

We display in figures 7 and 8 the same structure functions and angular coefficients as a function of the virtual photon invariant mass. Again, the calculation was done both for RHIC and the LHC, with the BK evolution and the DHJ model. We observe for the M dependence results that are qualitatively similar to what we already found for the k_{\perp} dependence. The DHJ model and the BK evolution are closer at the LHC rather than at RHIC. And again, we see that the suppression of the difference $W_{\Delta\Delta} - W_L/2$ compared to the “total” structure function W_{TL} is larger at large mass, or conversely that violations of the Lam-Tung relation are larger at small invariant mass.

4.3.3 Y dependence

Finally, we present results concerning the rapidity dependence, at fixed k_{\perp} and M , of the Drell-Yan structure functions and angular coefficients in figures 9 and 10. Note that the vertical scale in figure 9 is now linear, in order to better show the variations with Y and the differences between the BK evolution and the

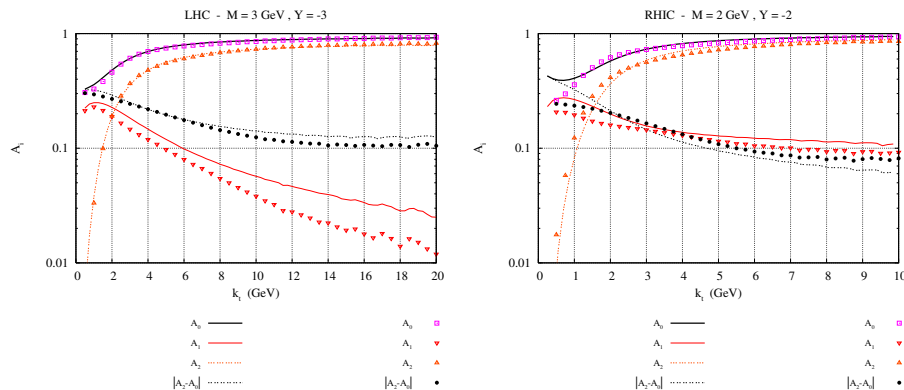


Figure 6: Angular coefficients as a function of k_{\perp} , for RHIC (right) and LHC (left). Lines: BK evolution. Points: DHJ model.

DHJ model. This natural makes the differences between the DHJ model and the BK evolution look larger than in the previous plots, while they are in fact comparable in magnitude.

Now, one sees qualitative differences between the two descriptions of the nuclear target. In absolute terms, the two descriptions do not differ by vast amounts, but the variations with Y are quite different. The general trend is that the BK evolution (with the parameters described in section 3.1) leads to significantly stronger variations with the rapidity. One should keep in mind that the DHJ model has been primarily devised to reproduce correctly the k_{\perp} dependence of the hadronic spectra observed by the BRAHMS and STAR collaborations at RHIC, and in particular their slope and how this slope varies with rapidity. However, it did not predict the absolute normalization of these spectra, and a “K-factor” had to be adjusted by hand. Moreover, the K-factor necessary to reproduce the normalization of the data turned out to be different at each rapidity. What we observe here may be related to this fact, and seems to indicate that the DHJ model should still be improved in order to get correctly the changes in the absolute normalization with rapidity.

Regardless of the description used for the function $C(\mathbf{l}_{\perp}, x_2)$ – BK evolution or DHJ model –, one also sees very different shapes at RHIC and the LHC. In the DHJ model, the slope tends to be inverted from RHIC to the LHC. And with the BK evolution, one goes from fairly symmetric shapes at RHIC to a very asymmetric rapidity distribution at the LHC. However, one should take this remark with caution, because our calculation of the Drell-Yan structure function treats the proton and the nucleus in very different ways, and is only valid when x_2 is small in the nucleus and x_1 is rather large in the proton. Therefore, the accuracy of our results at **positive rapidity** may suffer significantly from this treatment.

Finally, one can note that the violations of the Lam-Tung relation, that one

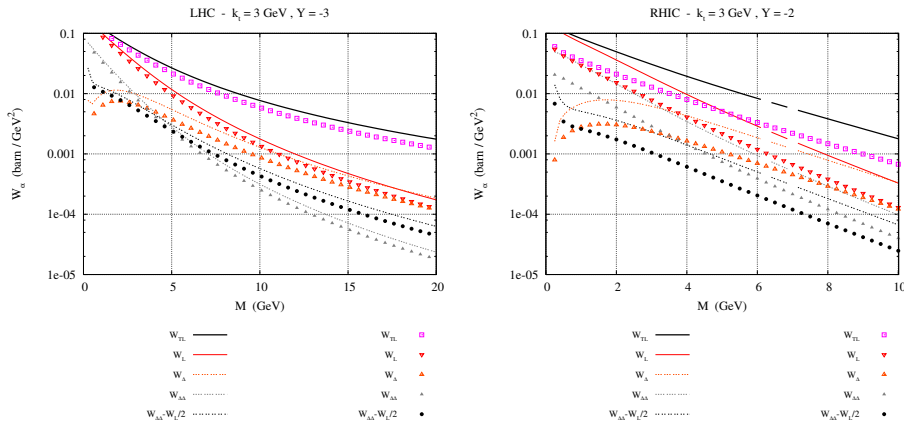


Figure 7: Drell-Yan structure functions as a function of M , for RHIC (right) and LHC (left). Lines: BK evolution. Points: DHJ model.

can see in figure 10 on the difference $A_0 - A_2$, rise steadily when the photon rapidity goes from positive to negative values (at least if one excludes the fragmentation regions of the two projectiles). This is also expected of a higher twist effect: indeed, at smaller y , i.e. at smaller x_2 , the density of color charges in the nucleus increases, which leads to more important rescattering effects.

5 Conclusions

In this paper, we have studied in the Color Glass Condensate framework the production of Drell-Yan pairs in proton-nucleus and deuteron-nucleus collisions at RHIC and at the LHC. Our treatment is asymmetric, because we only use the CGC description for the nucleus, while the proton or deuteron is described by means of the usual parton distributions.

All the nuclear effects that affect the Drell-Yan structure functions are encoded in the function $C(\mathbf{l}_\perp)$, which is the Fourier transform of the dipole-nucleus cross-section, and we have considered two descriptions of this object: the DHJ model and the solution of the BK equation (with the McLerran-Venugopalan model as the initial condition). Overall, the most striking differences between these two description are seen in the rapidity dependence of the structure functions, where the BK description leads to a much stronger rapidity dependence.

We have also discussed the Lam-Tung relation, a linear combination of the structure functions which is known to vanish identically up to (and including) the Next-to-Leading order in the leading twist approximation. Such a quantity is indeed very interesting to investigate in order to study the effects of higher twist contributions, because any non-zero value is by definition coming from higher twist. We observed for this quantity a behavior which is indeed what one

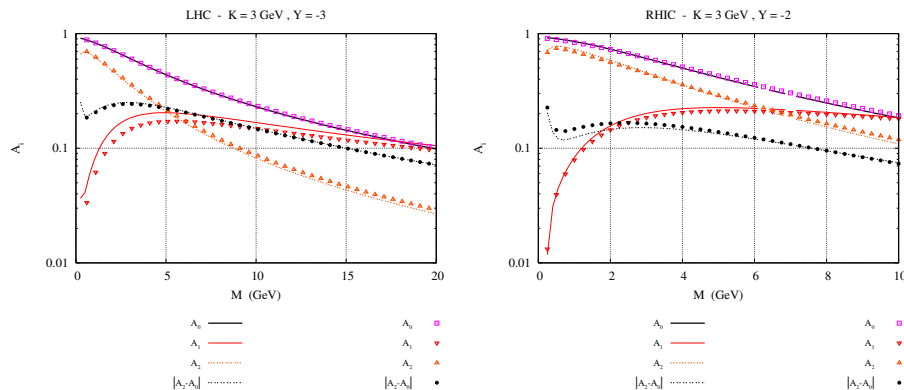


Figure 8: Angular coefficients as a function of M , for RHIC (right) and LHC (left). Lines: BK evolution. Points: DHJ model.

expects from a higher twist quantity: it drops at high momentum or high mass slightly faster than the total cross-section, and it is larger in regions of rapidity where the nucleus is probed at smaller x , i.e. where it has a larger parton density. A detailed experimental study of Lam-Tung relation then should prove very fruitful in advancing our knowledge of QCD in its novel high parton density regime.

Acknowledgements

F.G. would like to thank the hospitality of the Institute of Nuclear Theory where a significant part of this work has been performed, and the financial support of the grant ACTION CNRS-NSF #17251. J. J-M. is supported in part by the U.S. Department of Energy under Grant No. DE-FG02-00ER41132.

References

- [1] I. Arsene, et al., [BRAHMS collaboration] Phys. Rev. Lett. **93**, 242303 (2004).
- [2] E. Iancu, A. Leonidov, L.D. McLerran, Nucl. Phys. **A 692**, 583 (2001).
- [3] E. Iancu, A. Leonidov, L.D. McLerran, Phys. Lett. **B 510**, 133 (2001).
- [4] E. Ferreiro, E. Iancu, A. Leonidov, L.D. McLerran, Nucl. Phys. **A 703**, 489 (2002).
- [5] E. Iancu, R. Venugopalan, Quark Gluon Plasma 3, Eds. R.C. Hwa and X.N. Wang, World Scientific, hep-ph/0303204.

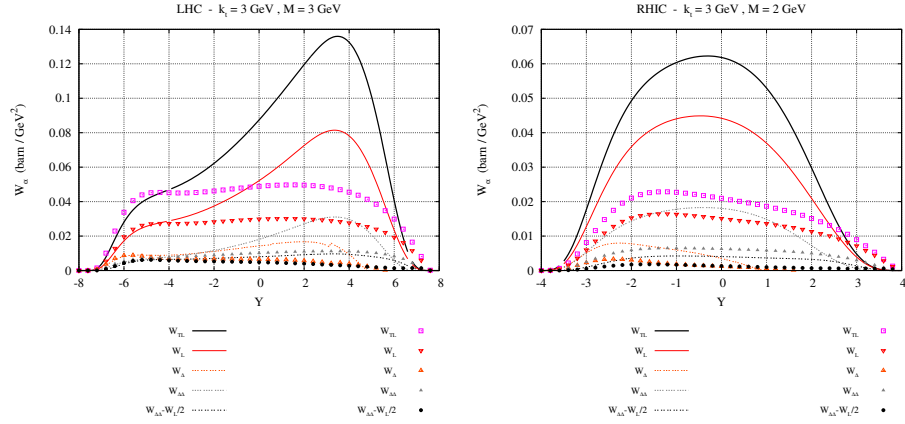


Figure 9: Drell-Yan structure functions as a function of Y , for RHIC (right) and LHC (left). Lines: BK evolution. Points: DHJ model.

- [6] D. Kharzeev, Yu. Kovchegov, K. Tuchin, Phys. Rev. **D 68**, 094013 (2003).
- [7] D. Kharzeev, Yu. Kovchegov, K. Tuchin, Phys. Lett. **B 599**, 23 (2004).
- [8] J. Jalilian-Marian, Nucl. Phys. **A 748**, 664 (2005).
- [9] A. Dumitru, A. Hayashigaki, J. Jalilian-Marian, Nucl. Phys. **A 765**, 464 (2006).
- [10] A. Dumitru, A. Hayashigaki, J. Jalilian-Marian, Nucl. Phys. **A 770**, 57 (2006).
- [11] Yu.V. Kovchegov, A.H. Mueller, Nucl. Phys. **B 529**, 451 (1998).
- [12] A. Kovner, U. Wiedemann, Phys. Rev. **D 64**, 114002 (2001).
- [13] Yu.V. Kovchegov, K. Tuchin, Phys. Rev. **D 65**, 074026 (2002).
- [14] A. Dumitru, L.D. McLerran, Nucl. Phys. **A 700**, 492 (2002).
- [15] A. Dumitru, J. Jalilian-Marian, Phys. Rev. Lett. **89**, 022301 (2002).
- [16] A. Dumitru, J. Jalilian-Marian, Phys. Lett. **B 547**, 15 (2002).
- [17] F. Gelis, J. Jalilian-Marian, Phys. Rev. **D 67**, 074019 (2003).
- [18] J.P. Blaizot, F. Gelis, R. Venugopalan, Nucl. Phys. **A 743**, 13 (2004).
- [19] F. Gelis, Y. Methar-Tani, Phys. Rev. **D 73**, 034019 (2006).
- [20] N.N. Nikolaev, W. Schafer, Phys. Rev. **D 71**, 014023 (2005).

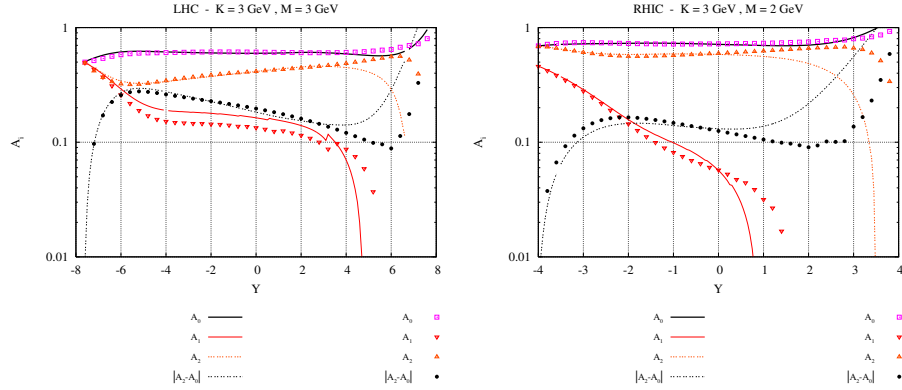


Figure 10: Angular coefficients as a function of Y , for RHIC (right) and LHC (left). Lines: BK evolution. Points: DHJ model.

- [21] J. Jalilian-Marian, Y. Kovchegov, *Prog. Part. Nucl. Phys.* **56**, 104 (2006).
- [22] J. Jalilian-Marian, A. Kovner, A. Leonidov, H. Weigert, *Nucl. Phys. B* **504**, 415 (1997).
- [23] J. Jalilian-Marian, A. Kovner, A. Leonidov, H. Weigert, *Phys. Rev. D* **59**, 014014 (1999).
- [24] J. Jalilian-Marian, A. Kovner, A. Leonidov, H. Weigert, *Phys. Rev. D* **59**, 034007 (1999).
- [25] J. Jalilian-Marian, A. Kovner, A. Leonidov, H. Weigert, *Erratum. Phys. Rev. D* **59**, 099903 (1999).
- [26] A. Kovner, G. Milhano, *Phys. Rev. D* **61**, 014012 (2000).
- [27] A. Kovner, G. Milhano, H. Weigert, *Phys. Rev. D* **62**, 114005 (2000).
- [28] J. Jalilian-Marian, A. Kovner, L.D. McLerran, H. Weigert, *Phys. Rev. D* **55**, 5414 (1997).
- [29] I. Balitsky, *Nucl. Phys. B* **463**, 99 (1996).
- [30] Yu.V. Kovchegov, *Phys. Rev. D* **61**, 074018 (2000).
- [31] R.C. Hwa, C.B. Yang, R.J. Fries, *Phys. Rev. C* **71**, 024902 (2005).
- [32] B.Z. Kopeliovich, J. Nemchik, I.K. Potashnikova, M.B. Johnson, I. Schmidt, *Phys. Rev. C* **72**, 054606 (2005).
- [33] J.W. Qiu, I. Vitev, *Phys. Lett. B* **632**, 507 (2006).
- [34] F. Gelis, J. Jalilian-Marian, *Phys. Rev. D* **66**, 014021 (2002).

- [35] F. Gelis, J. Jalilian-Marian, Phys. Rev. **D 66**, 094014, (2002).
- [36] J. Jalilian-Marian, Nucl. Phys. **A 753**, 307 (2005).
- [37] J. Jalilian-Marian, Nucl. Phys. **A 770**, 210 (2006).
- [38] D. D' Enterria, Private communication.
- [39] C.S. Lam, W.K. Tung, Phys. Lett. **B 80**, 228 (1979).
- [40] C.S. Lam, W.K. Tung, Phys. Rev. **D 21**, 2712 (1980).
- [41] C.S. Lam, W.K. Tung, Phys. Rev. **D 18**, 2447 (1978).
- [42] K. Rummukainen, H. Weigert, Nucl. Phys. **A 739**, 183 (2004).
- [43] E.A. Kuraev, L.N. Lipatov, V.S. Fadin, Sov. Phys. JETP **45**, 199 (1977).
- [44] I. Balitsky, L.N. Lipatov, Sov. J. Nucl. Phys. **28**, 822 (1978).
- [45] L.D. McLerran, R. Venugopalan, Phys. Rev. **D 49**, 2233 (1994).
- [46] L.D. McLerran, R. Venugopalan, Phys. Rev. **D 49**, 3352 (1994).
- [47] L.D. McLerran, R. Venugopalan, Phys. Rev. **D 50**, 2225 (1994).
- [48] A.M. Stasto, K. Golec-Biernat, J. Kwiecinski, Phys. Rev. Lett. **86**, 596 (2001).
- [49] F. Gelis, A. Stasto, R. Venugopalan, hep-ph/0605087.
- [50] S. Kretzer, H.L. Lai, F.I. Olness, W.K. Tung, Phys. Rev. **D 69**, 114005 (2004).